



**HAL**  
open science

## Influence of prestrain on mechanical properties of highly-filled Elastomers: Measurements and modeling

Anders Thorin, Aurélie Azoug, Andrei Constantinescu

### ► To cite this version:

Anders Thorin, Aurélie Azoug, Andrei Constantinescu. Influence of prestrain on mechanical properties of highly-filled Elastomers: Measurements and modeling. *Polymer Testing*, 2012, 10.1016/j.polymertesting.2012.07.014. 10.1016/j.polymertesting.2012.07.014 . hal-00723704v1

**HAL Id: hal-00723704**

**<https://polytechnique.hal.science/hal-00723704v1>**

Submitted on 13 Aug 2012 (v1), last revised 15 Jun 2016 (v2)

**HAL** is a multi-disciplinary open access archive for the deposit and dissemination of scientific research documents, whether they are published or not. The documents may come from teaching and research institutions in France or abroad, or from public or private research centers.

L'archive ouverte pluridisciplinaire **HAL**, est destinée au dépôt et à la diffusion de documents scientifiques de niveau recherche, publiés ou non, émanant des établissements d'enseignement et de recherche français ou étrangers, des laboratoires publics ou privés.

# Influence of prestrain on mechanical properties of highly-filled elastomers: Measurements and modeling

Anders Thorin<sup>a</sup>, Aurélie Azoug<sup>a</sup>, Andrei Constantinescu<sup>a</sup>

<sup>a</sup>Laboratoire de Mécanique des Solides - CNRS UMR 7649, École Polytechnique, 91128 Palaiseau Cedex, France

## Abstract

The prestrain influence on properties  $|E^*|$  and  $\tan(\delta)$  of four different HTPB composite propellants has been measured by Dynamic Mechanical Analyses (DMA). The non-linear behaviour observed has been modelled using a modified generalized Maxwell model. In order to describe the non-linearity, prestrain has been introduced as a variable of the stiffness of each Maxwell element using simple relations with two parameters. An algorithm was implemented to identify those parameters from the measurements. This paper presents the experimental results and the identification of the modified generalized Maxwell model parameters, as well as the simulated results. The influence of the relative weight between  $|E^*|$  and  $\tan(\delta)$  in the optimization process is exposed ???. It is shown that the dependence of the dynamic modulus on the uniaxial prestrain of the studied composite propellants can be described with few Maxwell elements and yet good accuracy.

*Key words:* composite propellants, HTPB, DMA, prestrain, generalized Maxwell model

## 1. Introduction

The modelling of the nonlinear viscoelastic mechanical behavior exhibited by these materials is either phenomenological (1; 2; 3) or requires a high level of homogenization and numerical implementation (4; 5; 6; 7; 8).

A particular experimental procedure is used, superimposing a tensile prestrain with small strain oscillations. This procedure has been previously discussed on unfilled rubber in tensile mode (9; 10), on filled elastomers with carbon black or silica fillers in tensile and shear mode (11; 12; 13; 14; 15; 16; 17) and on highly-filled elastomers in torsion mode (18).

**Model for influence of prestrain on DMA results, Morman, Lion, ??**

Composition of tested materials is presented in section 2. Section 3 describes experimental procedures. In section 4, the model of the non-linear behaviour is exposed and applied to the materials of section 2. The results and possible improvements are discussed.

## 2. Materials ??? (Aurélie a enlevé ce titre)

The four materials studied here are solid propellants, which are highly-filled elastomers. The materials differ from each other in filler fraction, NCO/OH ratio and plasticizer content as described in table 1.

Fillers are constituted of ammonium perchlorate and aluminium particles. The filler fraction varies between 86%wt and 90%wt. The binder is based on hydroxy-terminated polybutadiene (HTPB) prepolymer cured with

a methylene diisocyanate (MDCI). The quantity of MDCI compared to the quantity of polymer introduced is reflected by the NCO/OH ratio, which evolves from 0.8 to 1.1. The plasticizer introduced is dioctyl azelate (DOZ) molecules. Plasticizer content lies between 10%wt and 30%wt of the binder. The materials are thermally cured for 2 weeks at 50 °C.

| Material | Filler fraction (%wt) | NCO/OH ratio | Plasticizer (%wt binder) |
|----------|-----------------------|--------------|--------------------------|
| A        | 86                    | 0.80         | 10.0                     |
| B        | 88                    | 0.80         | 22.5                     |
| C        | 88                    | 0.95         | 30.0                     |
| D        | 90                    | 1.1          | 10.0                     |

Table 1: Materials studied

## 3. Experimental characterization

### 3.1. Experimental procedure

Dynamic Mechanical Analysis (DMA) experiments are achieved using a Metravib Viscoanalyseur VA3000. The experimental procedure consists in superimposing a tensile prestrain and a sinusoidal strain. The total strain is

$$\varepsilon(t) = \varepsilon_0 + \varepsilon_a \sin(\omega t), \quad (1)$$

where  $\varepsilon_a = 0.01\%$  and  $\omega = 2\pi f$ . The frequency  $f$  is fixed at 5Hz. The tests are performed at room temperature. Different levels of prestrain  $\varepsilon_{0,i}$  are reached as illustrated on

figure 1, from 0.01% to about 10%. In some cases, final failure of the specimen is reached at lower prestrain than 10%.

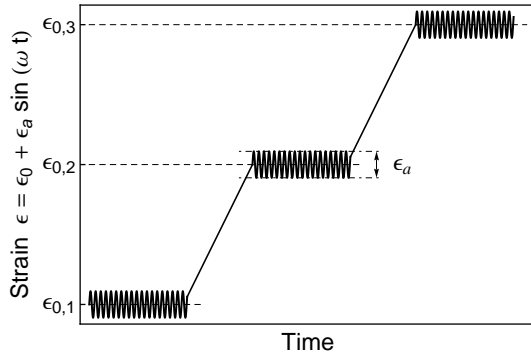


Figure 1: Schematic representation of the strain history during a prestrained DMA experiment

Norm of complex modulus  $|E^*|$  and loss factor  $\tan \delta$  are measured (??? define complex modulus???). The storage and loss moduli  $E'$  and  $E''$  are deduced from these measurements using equations (2) or (3). EST-CE QUE E' ET E'' NE SONT PAS TOUJOURS POSITIFS ???

$$E' = |E^*| \cos \delta, \quad E'' = |E^*| \sin \delta, \quad (2)$$

or their inverse relations

$$|E^*| = \sqrt{E'^2 + E''^2}, \quad \tan \delta = \frac{E''}{E'}. \quad (3)$$

The storage modulus  $E'$  quantifies the elastic part of the behaviour while the loss modulus  $E''$  corresponds to the quantity of heat dissipated by friction between polymer chains during a strain cycle (19).

### 3.2. Results and discussion

The aim is to determine the influence of prestrain on the viscoelastic behaviour, quantified by the parameters ( $|E^*|, \tan \delta$ ) or equivalently ( $E', E''$ ). All propellants exhibit a three-phase behaviour: a linear domain, a transition phase and a nonlinear domain (???is the transition phase linear???), as shown on figures 2 and 3. The linear domain corresponds to the plateau at low prestrain where the viscoelastic properties do not evolve according to prestrain  $\varepsilon_0$ . The transition phase appears at a prestrain of approximately 1% and a nonlinearity threshold is observed. Finally, the nonlinear domain is the part of the curve where the viscoelastic properties evolve linearly with the logarithmic prestrain. In the nonlinear domain, storage and loss moduli  $E'$  and  $E''$  increase as prestrain  $\varepsilon_0$  increases.

The measurements obtained for materials A to D show that material composition has a great influence on linear

and nonlinear behaviours. The values of the moduli  $E'$  and  $E''$  in the linear domain are directly dependent on filler fraction. Moreover, the comparison between materials B and C shows that NCO/OH ratio and plasticizer content modify the viscoelastic behaviour, especially the dissipations quantified by  $E''$  (figure 3). Indeed, the role of plasticizer molecules is to diminish friction between polymer chains into the microstructure. Consequently, an increase of plasticizer content leads to a decrease of the measured  $E''$ .

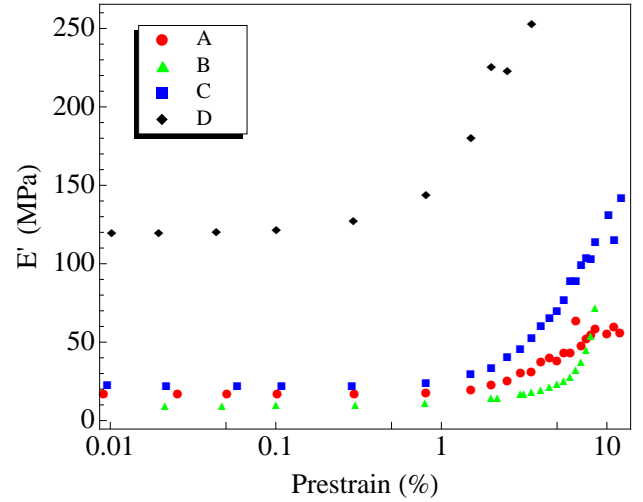


Figure 2: Comparison of materials A to D, storage modulus  $E'$  vs prestrain  $\varepsilon_0$ , with  $\varepsilon_a = 0.01\%$

|   | Linear domain |       | Thresholds |       | Slopes |       |
|---|---------------|-------|------------|-------|--------|-------|
|   | $E'$          | $E''$ | $E'$       | $E''$ | $E'$   | $E''$ |
| A | 17.4          | 8.3   | 1.02       | 1.20  | 58.6   | 7.9   |
| B | 6.7           | 6.7   | 1.12       | 1.29  | 76.9   | 10.5  |
| C | 21.9          | 8.4   | 0.98       | 1.18  | 126.5  | 14.6  |
| D | 118.5         | 28.8  | 0.03       | 0.26  | 663.5  | 82.4  |

Table 2: Values characterizing the linear domain, the transition phase and the nonlinear domain for propellants A to D

The initiation of the nonlinearity is commonly associated with the maximal extensibility of the network (14; 15; 16). This material characteristic depends on filler fraction, NCO/OH ratio and plasticizer content. The storage and loss moduli nonlinearity thresholds are reached at prestrains globally decreasing with increasing filler fraction from material A to material D, see table 2. The presence of fillers also induces strain amplification (20) which could explain the predominant influence of filler fraction on these values.

Moreover, materials B and C contain the same fraction of fillers and present different thresholds. The main

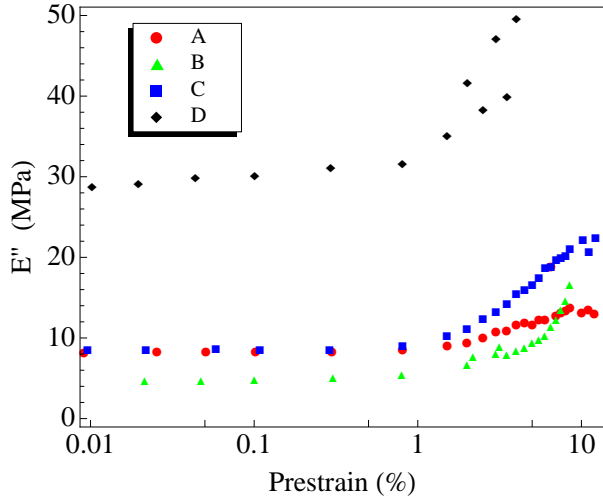


Figure 3: Comparison of materials A to D, loss modulus  $E''$  vs prestrain  $\varepsilon_0$ , with  $\varepsilon_a = 0.01\%$

difference between the two propellants is the NCO/OH ratio, see table 1. Indeed, as the NCO/OH ratio increases, the network cross-linking density increases, the mesh size decreases, and consequently the threshold decreases. Finally, since material A threshold is lower than the one measured for material B, it appears that the influence of fillers on the maximal extensibility of the network is counteracted by the influence of plasticizer content. Plasticizer molecules facilitate movements into the microstructure and hence increase the network maximal extensibility.

The slopes of the storage and loss moduli are determined from the experimental measurements, see table 2. Both values increase with increasing filler fraction as a direct effect of strain amplification. The microstructure mechanism leading to the measured nonlinearity is also linked to fillers organization (21). Additionally, the slopes increase when NCO/OH ratio increases. Considering the high filler fraction introduced in propellants, it is well known that the local strain is highly heterogeneous. Consequently, the network maximal extensibility is not uniformly reached in every part of the microstructure at a unique prestrain. The slope is then a quantification of the rate at which the maximally extended part of the network increases with prestrain. This value depends logically on NCO/OH ratio as well as filler fraction.

The measured nonlinear behaviour also depends on the single strain amplitude  $\varepsilon_a$  value, as shown in figures 4 and 5 for material B. In the linear domain, the storage and loss moduli decrease as  $\varepsilon_a$  increases. The nonlinearity thresholds are higher and the slopes decrease as the strain amplitude increases.

In spite of the absence here of a maximum on the  $E''$  curve, characteristic of the Payne effect, this behaviour

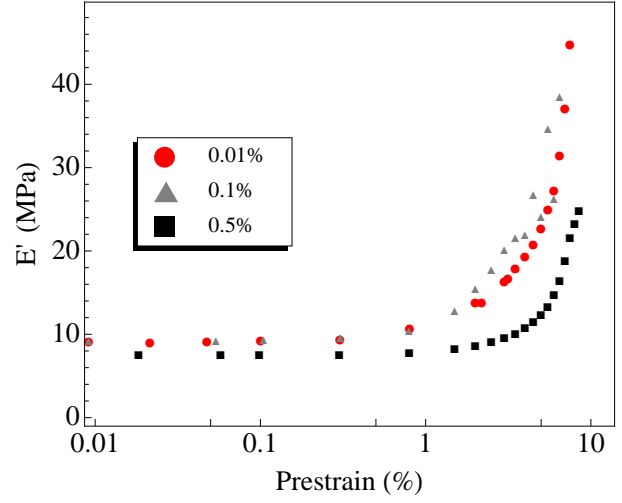


Figure 4: Influence of strain amplitude  $\varepsilon_a$  on nonlinearity in  $E'$ , material B.

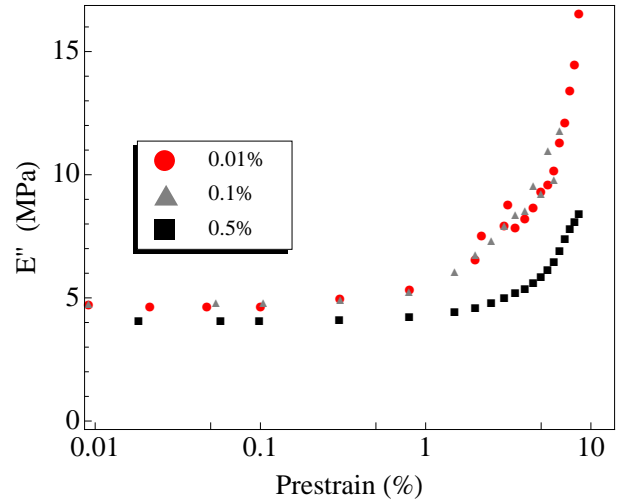


Figure 5: Influence of strain amplitude  $\varepsilon_a$  on nonlinearity in  $E''$ , material B.

is well known and specific to filled elastomers (22). It is generally associated to the behaviour of a filler network, which is destroyed and reagglomerated according to strain oscillation at a rate depending on strain amplitude (23). The existence of a filler network is yet to be proved in highly-filled elastomers such as propellants since the chemical nature of the fillers does not necessarily involve a strong reinforcement action between the filler surface and the polymeric binder (24; 25).

It is however supposed that since the filler fraction

is particularly high, the fillers organization into the microstructure has a strong effect on the mechanical behaviour. Hence, a high amplitude strain oscillation allows microstructural movements which lead to a more uniform strain field. The prestrain at which part of the network reaches maximal extensibility is then increased while the nonlinearity slope decreases.

Although the measured nonlinearity is quantitatively dependent on material composition and strain amplitude  $\varepsilon_a$ , the observed behaviour is qualitatively identical. This means that a model developed for one propellant and one measurement could easily be fitted to any other one, involving only quantitative modifications.

#### 4. Modeling of the nonlinear behaviour

The generalized Maxwell model is often used to model viscoelastic material behaviour (26). The objective here is to modify this model in order to take into account the influence of the prestrain  $\varepsilon_0$  on the response measured by  $|E^*|$ ,  $\tan(\delta)$  or equivalently  $E'$ ,  $E''$ .

##### 4.1. Generalized Maxwell model

The generalized Maxwell model and the notations are represented on figure 6.

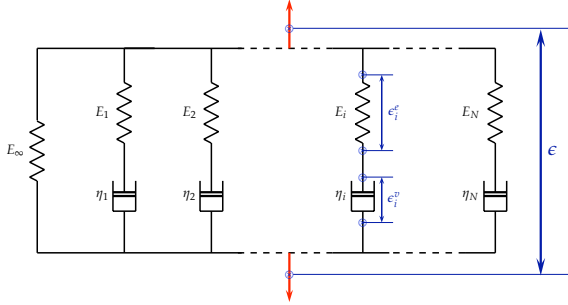


Figure 6: Generalized Maxwell model with  $N$  viscoelastic elements

Each viscoelastic element is represented by its stiffness  $E_i$  and its viscosity  $\eta_i$  ( $i = 1, N$ ). The characteristic time of each Maxwell element is defined by:  $\tau_i = \eta_i/E_i$ . The stress is related to the strain history by the following expression:

$$\sigma(t) = \int_{-\infty}^t \left( E_{\infty} + \sum_{i=1}^n E_i e^{-\frac{t-s}{\tau_i}} \right) \dot{\varepsilon}(s) ds. \quad (4)$$

The continuous spectrum of relaxation times of the materials is described in a generalized Maxwell model by the set of characteristic times  $(\tau_1, \dots, \tau_N)$ , which is supposed to be a priori fixed. The stiffnesses  $E_i$  are identified from the experimental data.

In order to introduce the influence of prestrain, we assume that the stiffness of the different viscoelastic Maxwell elements are a function of prestrain:

$$E_i = E_i(\varepsilon_0).$$

We shall consider two types of linear dependence of the stiffness with prestrain, either of the form:

$$E_i(\varepsilon_0) = f_i(\varepsilon_0) \quad \text{with} \quad f_i(\varepsilon_0) = a_i \varepsilon_0 + b_i$$

or of the form:

$$E_i(\varepsilon_0) = g_i(\varepsilon_0) \quad \text{with} \quad g_i(\varepsilon_0) = \begin{cases} 0 & \text{if } \varepsilon_0 \leq c_i \\ a_i(\varepsilon_0 - c_i) & \text{if } \varepsilon_0 > c_i \end{cases}$$

as illustrated in figure 7. The parameters of the two models,  $p_i = (a_i, b_i)$  and  $p_i = (a_i, c_i)$  respectively, are real positive constants. One can remark that the element  $i$  defined by  $E_i = g$  has a vanishing stiffness if the prestrain is smaller than  $c_i$  and can be considered to be inactive in the model representation.

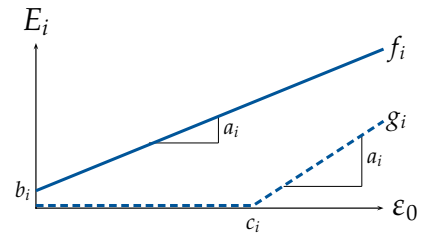


Figure 7: Dependence of the stiffness  $E_i$  of the viscoelastic element  $i$  on the prestrain  $\varepsilon_0$

As the characteristic times  $\tau_i$  are considered to be a priori fixed, it implies that the viscosities  $\eta_i$  evolve with prestrain in order to keep the ratio  $\tau_i = \eta_i/E_i$  constant.

The objective is to determine a modified generalized Maxwell model which will fit the evolutions in terms of prestrain of  $E^*$  and  $\tan \delta$  or  $E'$  and  $E''$ .

Let us further assume that we dispose of a series of measurements of  $(|E^*|, \tan \delta)$  for  $K$  increasing prestrain levels:  $\varepsilon_{0_1} < \dots < \varepsilon_{0_k} < \dots < \varepsilon_{0_K}$ .

The modified generalized Maxwell model will be constructed the following way. We start from a model with only two viscoelastic elements with a stiffness of the form  $f$ . The parameters representing the stiffness are identified in a step-by-step procedure taking the experimental values for larger and larger prestrain levels into account. First the results for the smallest prestrain are used, then the next larger one is included, finishing with all prestrain levels.

If the identification fails to reach desired tolerance, a new viscoelastic element with a stiffness of the form  $g$  is added and the identification procedure of the parameters is restarted from the beginning.

The complete algorithm is detailed hereafter, where  $K$  is the total number of strain levels, i.e. of measurements.

i) Initial step:

$n = 2$  viscoelastic elements

$$E_i = f_i \quad i = 1, n$$

$k = 2$  prestrain levels

ii) STEP 1

Find parameters  $\{p_i \mid 1 \leq i \leq n\}$  by minimizing  $\mathcal{J}$

STEP 2:  $\mathcal{J} < TOL?$

FALSE

$n = n + 1$

Add new viscoelastic element

$E_n = g_n$  with  $c_n = \varepsilon_{0k}$ .

GO TO STEP 1

TRUE

IF  $k = K$  STOP

ELSE

$k = k + 1$

Add new series of prestrain

GO TO STEP 1

#### 4.2. Identification Procedure

The cost function  $\mathcal{J}$  has been defined in terms of computed and measured complex modulus and loss factor by the following expression:

$$\mathcal{J} = \frac{\| |E^*|^c - |E^*|^m \|^2}{\| |E^*|^m \|^2} + \alpha \frac{\| \tan(\delta)^c - \tan(\delta)^m \|^2}{\| \tan(\delta)^m \|^2}$$

where  $\cdot^c$  and  $\cdot^m$  denote the computed and measured quantities respectively. The definitions of  $|E^*|$  and  $\tan \delta$  applied to the generalized Maxwell model leads to the expressions used to calculate  $|E^*|^c$  and  $\tan(\delta)^c$  in the cost function:

$$\begin{cases} |E^*|^c = \left[ \left( E_\infty + \sum_{i=1}^n \frac{(2\pi f \tau_i)^2}{1+(2\pi f \tau_i)^2} E_i \right)^2 + \left( \sum_{i=1}^n \frac{2\pi f \tau_i}{1+(2\pi f \tau_i)^2} E_i \right)^2 \right]^{\frac{1}{2}} \\ \tan(\delta)^c = \left( \sum_{i=1}^n \frac{2\pi f \tau_i}{1+(2\pi f \tau_i)^2} \right) \cdot \left( E_\infty + \sum_{i=1}^n \frac{2\pi f \tau_i}{1+(2\pi f \tau_i)^2} E_i \right)^{-1} \end{cases}$$

The norm  $\| \cdot \|$  is the standard vector distance in  $\mathbb{R}^k$ , where  $k$  is the maximum number of prestrain values under consideration. More precisely, the first  $k$  measurements of the complex modulus are:

$$|E^*|^m = [|E^*|(\varepsilon_{01}) \dots |E^*|(\varepsilon_{0k})]^T$$

and the norm is given as:

$$\| |E^*|^m \| = \sqrt{|E^*|(\varepsilon_{01})^2 + \dots + |E^*|(\varepsilon_{0k})^2}.$$

$\alpha$  is a real constant and denotes the relative weight between the errors in complex modulus and loss factor, and has been taken equal to 1.

**This discussed later (???)**.

The identification algorithm was implemented into MATHEMATICA<sup>®</sup>. The optimisation algorithm gave the best results with an automatic detection of the numerical method. The following section illustrates the results obtained on materials A, B, C and D.

#### 4.3. Results and discussion

$E_\infty$  has been experimentally determined on material B and is equal to 3.31 MPa. The same value has been used for all four materials. The series of characteristic times  $\tau_i$  has been chosen as  $10^{i-2}$ s. Therefore the two initial Maxwell elements 1 and 2 have characteristic times of respectively  $10^{-2}$ s and  $10^{-1}$ s.

##### 4.3.1. Identified stiffnesses and output in $|E^*|, \tan(\delta)$

The experimental measurements for material B with strain amplitude  $\varepsilon_a = 0.01\%$  is shown on figure 8, as well as the model response  $|E^*|$  and  $\tan(\delta)$  identified with the previously described procedure. The corresponding identified stiffness  $E_i$  are shown on figure 9. They are equivalently defined by the identified parameters  $a_i, b_i, c_i$  of table 3.

Three different steps of the procedure are represented. The first one corresponds to the identification on the first 5 measurements with a prestrain level up to 0.30%, which requires only the two first Maxwell elements of the model, the tolerance being fixed at 0.005. The second step considered takes into account the first 9 measurements where  $\varepsilon_0$  reaches 3.1% and the third element is still not activated ( $a_3 = 0$ MPa,  $c_3 = 0$ ). At the final step,  $\varepsilon_{0,\max} = 6.0\%$  and 3 elements are required so that the model describes the measured behaviour on the first 16 measurements. With the measurement corresponding to the 17th prestrain level, the cost function value is higher than the tolerance (of 0.05). Therefore, in accordance with the algorithm, a fourth Maxwell element has to be taken into account. The present implementation of the procedure was not able to produce correct identified values for all four elements, due to numerical divergence (???)

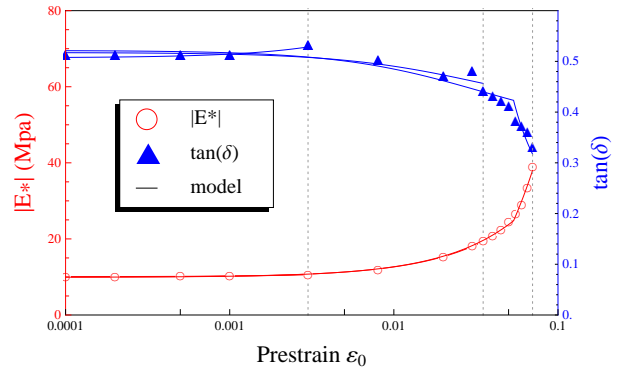


Figure 8: Model response with stiffnesses of figure 9 in  $|E^*|, \tan(\delta)$ , compared with the measurement, material B,  $\varepsilon_a = 0.01\%$

#### AJUSTER LES DEUX COURBES

The response of the same identified model can be plotted in  $E', E''$  using relations 2. The following figures are plotted in  $E', E''$  since it is easier to interpret ???. Figure 8 is redrawn on figure 10. The relative error in  $E'$  is then

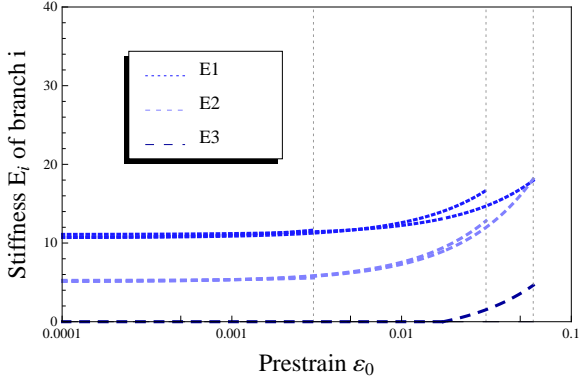


Figure 9: Identified stiffnesses at three different steps, material B,  $\varepsilon_a = 0.01\%$

| $\varepsilon_0$ | $a_1$<br>(MPa) | $b_1$<br>(MPa) | $a_2$<br>(MPa) | $b_2$<br>(MPa) | $a_3$<br>(MPa) | $c_3$  |
|-----------------|----------------|----------------|----------------|----------------|----------------|--------|
| 0.0030          | 315.3          | 10.7           | 106.5          | 5.2            |                |        |
| 0.0314          | 190.7          | 10.7           | 245.6          | 5.1            |                |        |
| 0.0597          | 115.06         | 11.1           | 218.6          | 5.1            | 110.1          | 0.0176 |

Table 3: Identified parameters of stiffnesses  $E_i$  for material B, plotted on figure 9

of 0.35% for step 1, 1.41% for step 2, and 1.97% for the last step. In other words, the identified model applied to material B with  $\varepsilon_a = 0.01\%$  and strains up to 6.0% describes what has been measured with an relative error of less than 2% in  $E'$ .

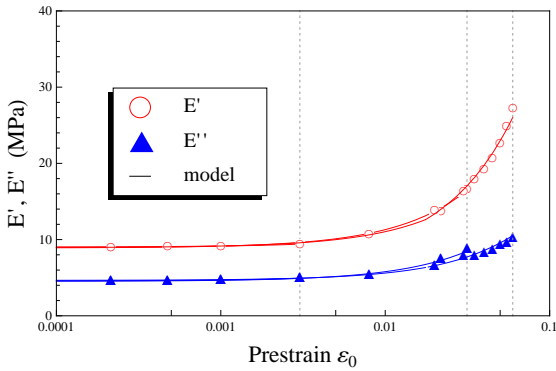


Figure 10: Model response with stiffnesses of figure 9 in  $E', E''$

#### 4.3.2. Identification results in $E', E''$ for materials A,C,D

The identification procedure has also been tested on materials A, C and D and the results are respectively represented on figure 11, 12 and 13. The relative errors in  $E'$  for the last steps are respectively 3.5%, 1.1% and 2.99%. It has to be mentioned that these results were not obtained with the same value of the tolerance which appears in the algorithm as described previously. This point is discussed later in this section.

The exposed results show that the procedure can generate models which describe the measurements on mate-

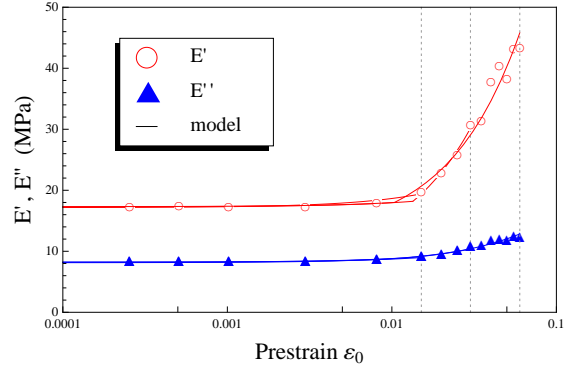


Figure 11: Response in  $E', E''$  of the identified model for material A,  $\varepsilon_a = 0.01\%$

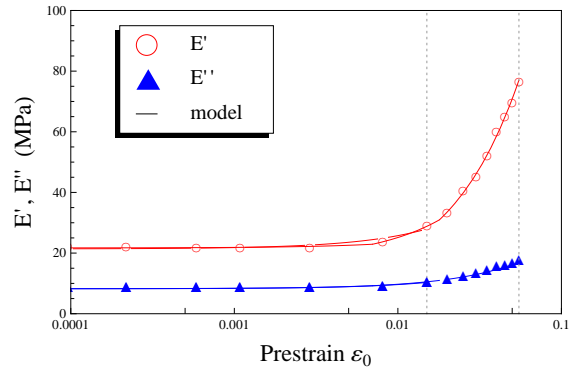


Figure 12: Response in  $E', E''$  of the identified model for material C,  $\varepsilon_a = 0.01\%$

rial A, B, C and D with a maximum relative error of 3.5% when  $\varepsilon_a = 0.01\%$  ( $\varepsilon$  maximal ???) Erreur en  $E''$  ???.

#### 4.3.3. Identification results with different $\varepsilon_a$

The algorithm has also been used to describe behavior of material B with different strain amplitudes  $\varepsilon_a$ . The results with  $\varepsilon_a = 0.01\%$  have been shown on figure 10. Figure 14 represents the response of the identified model for  $\varepsilon_a = 0.1\%$  and figure 15 the response for  $\varepsilon_a = 0.5\%$ . The relative errors in  $E'$  are respectively 2.56% and 1.27% (1.97% with  $\varepsilon_a = 0.01\%$  as said previously).

#### 4.3.4. Self-adaptiveness

The procedure automatically activates additional elements when the cost function is higher than the given tolerance. For example, with a tolerance of 0.005 for the measurements of material B and a strain amplitude of  $\varepsilon_a = 0.1\%$ , the cost function reaches 0.016  $>$  0.005 for the model with two elements and the eight first prestrain levels taken into account. The relative error in  $E'$  is 3.58%. Therefore the procedure activates an additional Maxwell element. The new identified parameters of the three elements fit to the measurements with a relative error of 0.36% for the same eight prestrain levels. This illustrates the power of the algorithm, the main obstacle being that

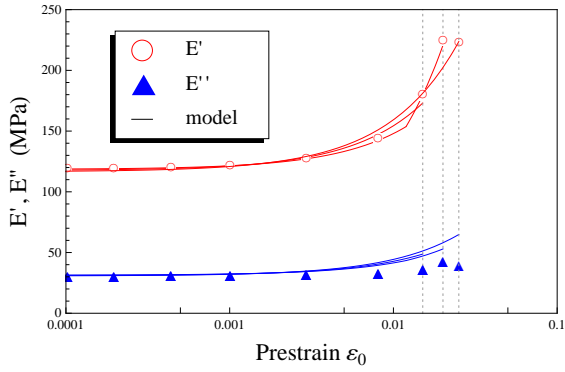


Figure 13: Response in  $E'$ ,  $E''$  of the identified model for material D,  $\varepsilon_a = 0.01\%$

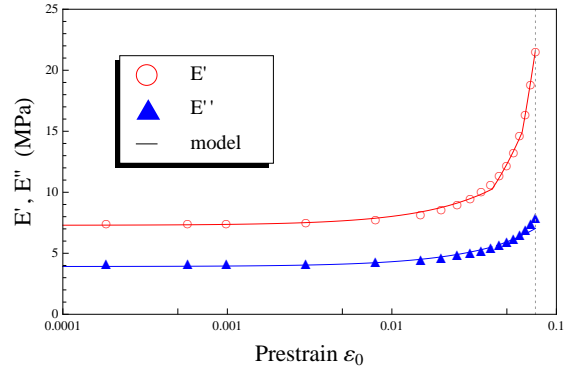


Figure 15: Response in  $E'$ ,  $E''$  of the identified model for material B,  $\varepsilon_a = 0.5\%$

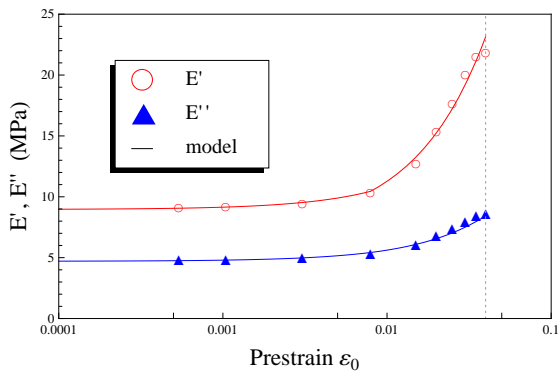


Figure 14: Response in  $E'$ ,  $E''$  of the identified model for material B,  $\varepsilon_a = 0.1\%$

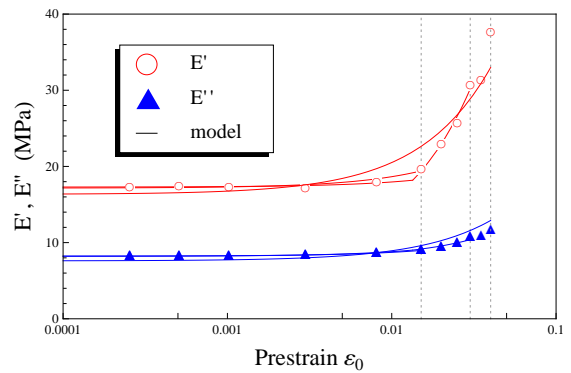


Figure 16: Response in  $E'$ ,  $E''$  of the identified model for material A, tolerance divided by 2.5 compared to figure 11,  $\varepsilon_a = 0.01\%$

the identification do not always converge with more than three elements.

#### 4.3.5. Sensitivity to tolerance

The tolerance used in the identification algorithm described in section 4 has to be chosen carefully. In case of noisy measurements, better results can be obtained by increasing the tolerance. For example, figure 11 was obtained with a tolerance of 0.05 whereas figure 16 was generated with a tolerance of 0.02. RELATIVE ERRORS ??? If the tolerance is too low, the algorithm will not be able to fit precisely enough the noisy measurements. Once it is increased, it may produce a description with a sufficiently low relative error in  $E'$  (3.5% for material A).

#### 4.3.6. Remarks

Other sensitivities have been tested. It appears that multiplying  $E_\infty$  by 10 or 0.1 results in a significant loss of quality and may lead the non-convergence of the optimisation. The same observations can be done when the relaxation times  $\tau_1$  are chosen 10 times greater or lower. These parameters  $E_\infty$  and  $\tau_i$  could theoretically be integrated into the cost function variable but it would increase the numerical stiffness (??) and the parameters identification would get even more complex (??).

Nevertheless, when  $E_\infty$ ,  $\tau_1$  and the tolerance were correctly fixed, the procedure identified models which fit to the experiments with relative errors lower than 3.5% and for strains up to 6%, for all materials A, B, C, D and for all three strain amplitude of material B.

It has to be noticed that the relative error is calculated from the measurements, and therefore that it is not possible to calculate a continuous relative error. In other words, there is no possible verification of the accuracy of the model between to measurements. (???)

The number of elements adapts automatically. The identification procedure takes only a few seconds a commercialized computer. It may not converge for some elements ( $i > 3$ ) but produces a model which describes the observation up to reasonably high strains (at least ?? on all tests performed) with relatively accurate results (maximum relative error of 3.5% on all performed tests). The model parameters need to be identified from measurements. They depend on the material and the strain amplitude, thus it is not a global model of the behavior of highly-filled elastomers.

## 5. Conclusion

Prestrain produces a nonlinear behavior of highly-filled elastomers. This nonlinearity has been measured and is discussed on four different HTBP composite propellants. A generalized Maxwell model was used to simulate the behavior. Its relaxation times have been fixed and its constant stiffnesses changed to simple functions of two parameters each. The article expose the procedure which identify those parameters. The number of elements to be taken into account automatically changes when needed. For all four materials and three different strain amplitudes, simple models were identified. They simulate the observations with relative error inferior to 3.5% for prestrains up to 6%. For greater prestrains and same tolerance, new Maxwell elements have to be considered but the algorithm did not manage to identify their parameters. Therefore the model is not always valid for all prestrains.

## Acknowledgements

## References

- [1] S. Ozupek, E. Becker, Constitutive modeling of high-elongation solid propellants, *J. Eng. Mater. Technol.-Trans. ASME* 114 (1) (1992) 111–115.
- [2] S. Ozupek, E. Becker, Constitutive equations for solid propellants, *J. Eng. Mater. Technol.-Trans. ASME* 119 (1997) 125–132.
- [3] G. Ravichandran, C. Liu, Modeling constitutive behavior of particulate composites undergoing damage, *Int. J. Solids Struct.* 32 (1995) 979–990.
- [4] C. Nadot-Martin, H. Trumel, A. Dragon, Morphology-based homogenization for viscoelastic particulate composites. Part I: Viscoelasticity sole, *Eur. J. Mech. A-Solid* 22 (1) (2003) 89–106.
- [5] C. Nadot-Martin, A. Dragon, H. Trumel, A. Fanget, Damage modelling framework for viscoelastic particulate composites via a scale transition approach, *J. Theor. Appl. Mech.* 44 (3) (2006) 553–583.
- [6] C. Nadot-Martin, M. Touboul, A. Dragon, A. Fanget, Chapter 12. Direct scale transition approach for highly-filled viscohyperelastic particulate composites: computational study, *ISTE/Wiley*, 2008, pp. 218–237.
- [7] F. Xu, N. Aravas, P. Sofronis, Constitutive modeling of solid propellant materials with evolving microstructural damage, *J. Mech. Phys. Solids* 56 (2008) 2050–2073.
- [8] K. Matous, H. Inglis, X. Gu, D. Rypl, T. Jackson, P. Geubelle, Multi-scale modeling of solid propellants: From particle packing to failure, *Compos. Sci. Technol.* 67 (2007) 1694–1708.
- [9] P. Mason, The viscoelastic behavior of rubber in extension, *J. Appl. Polym. Sci.* 1 (1) (1959) 63–69.
- [10] J. Davies, A. Thomas, K. Akutagawa, The effect of low molar mass liquids on the dynamic mechanical properties of elastomers under strain, *Prog. Rubber Plastics Technol.* 12 (3) (1996) 174–190.
- [11] E. Meinecke, S. Maksin, Influence of large static deformation on the dynamic properties of polymers. Part II influence of carbon black loading, *Rubber Chem. Technol.* 54 (1981) 857–870.
- [12] J. Sullivan, V. Demery, The nonlinear viscoelastic behavior of a carbon black-filled elastomer, *J. Polym. Sci. Pol. Phys. Ed.* 20 (1982) 2083–2101.
- [13] K. Arai, J. Ferry, Differential dynamic shear moduli of various carbon-black-filled rubbers subjected to large step shear strains, *Rubber Chem. Technol.* 59 (1986) 605–614.
- [14] A. Voet, J. Morawski, Dynamic mechanical and electrical properties of vulcanizates at elongations up to sample rupture, *Rubber Chem. Technol.* 47 (1974) 765–777.
- [15] N. Dutta, D. Tripathy, Influence of large static deformations on the dynamic mechanical properties of bromobutyl rubber vulcanizates : Part I. Effect of carbon black loading, *Polym. Test.* 9 (1990) 3–13.
- [16] J. Busfield, C. Deeprasertkul, A. Thomas, The effect of liquids on the dynamic properties of carbon black filled natural rubber as a function of pre-strain, *Polymer* 41 (2000) 9219–9225.
- [17] R. Warley, D. Feke, I. Manas-Zloczower, Transient effects in dynamic modulus measurement of silicone rubber, Part 2: Effect of mean strains and strain history, *J. Appl. Polym. Sci.* 104 (2007) 2197–2204.
- [18] A. Adicoff, A. Lepie, Effect of tensile strain on the use of the WLF equation, *J. Appl. Polym. Sci.* 14 (1970) 953–966.
- [19] A. Medalia, Effect of carbon black on dynamic properties of rubber vulcanizates, *Rubber Chem. Technol.* 51 (1978) 437–523.
- [20] L. Mullins, N. Tobin, Stress softening in rubber vulcanizates. Part I. Use of a strain amplification factor to describe the elastic behavior of filler-reinforced vulcanized rubber, *J. Appl. Polym. Sci.* 9 (1965) 2993–3009.
- [21] A. Azoug, Micromécanismes et comportement macroscopique d'un élastomère fortement chargé, Ph.D. thesis, Ecole Polytechnique (2010).  
URL <http://tel.archives-ouvertes.fr/tel-00552234/fr/>
- [22] A. Payne, The dynamic properties of carbon black-loaded natural rubber vulcanizates. Part I, *J. Appl. Polym. Sci.* VI (1962) 57–63.
- [23] G. Kraus, Mechanical losses in carbon-black-filled rubbers, *J. Appl. Polym. Sci. : Applied Polymer Symposium* 39 (1984) 75–92.
- [24] R. Stacer, C. Hubner, D. Husband, Binder/filler interaction and the nonlinear behavior of highly-filled elastomers, *Rubber Chem. Technol.* 63 (1990) 488–502.
- [25] R. Stacer, D. Husband, Small deformation viscoelastic response of gum and highly filled elastomers, *Rheol. Acta* 29 (1990) 152–162.
- [26] R. Christensen, *Theory of viscoelasticity: An Introduction*, Academic Press, New York, 1971.